ECS Journal of Solid State Science and Technology, 2020 **9** 015018

Nitride LEDs and Lasers with Buried Tunnel Junctions

Henryk Turski,[1,z] Marcin Siekacz,[1] Grzegorz Muzioł,[1] Mateusz Hajdel,[1] Szymon Stańczyk,[1] Mikołaj Żak,[1] Mikołaj Chlipała,[1] Czeslaw Skierbiszewski,[1] Shyam Bharadwaj,[2] Huili Grace Xing,[2] and Debdeep Jena[2]

[1]*Institute of High Pressure Physics, Polish Academy of Sciences, 01-142 Warsaw, Poland*
[2]*Cornell University, Ithaca, New York 14850, USA*

Traditionally, Nitride semiconductors have suffered from poor p-type conductivity, requiring Mg activation by removing hydrogen from grown layers either through thermal annealing or electron irradiation. This requirement restricts the growth of buried p-type layers. Here, we report structures obtained using a Hydrogen-free growth technique – plasma assisted molecular beam epitaxy. Using this method, top and bottom tunnel junctions are realized for top and bottom contacts to traditional Ga-polar devices. Advantages of using both constructions are discussed. The efficiency of the bottom-tunnel junction design is presented through realization of a stable laser diode operating at room temperature. Further work needed to improve tunnel junction performance as well as optical mode confinement to fully benefit from this design is outlined.

 [DOI: 10.1149/2.0412001JSS]

Manuscript submitted September 20, 2019; revised manuscript received October 18, 2019. Published December 5, 2019. *This paper is part of the JSS Focus Issue on Recent Advances in Wide Bandgap III-Nitride Devices and Solid State Lighting: A Tribute to Isamu Akasaki.*

The interest in research devoted to Gallium Nitride and related compounds was triggered by an abundance of applications for electronic and optoelectronic devices. One of the key application is the general lighting, which is realized with visible light emitting diodes (LEDs) based on Gallium Nitride. This invention led to the awarding of the Nobel Prize to Professor Isamu Akasaki, Professor Hiroshi Amano and Professor Shuji Nakamura.[1–3] Another distinguishing feature of the Nitride semiconductors compared to traditional III-V and group-IV semiconductors is the presence of built-in electric fields. By changing the chemical composition and strain in epitaxial layers, one can control the magnitude of both the spontaneous and piezoelectric components of the electronic polarization. In addition, one can also use substrates of various crystallographic orientations to tune the polarization field.

In many cases, however, changing the substrate orientation from Ga-polar to either N-polar, non-polar or semi-polar results in undesired features such as dislocation propagation or point defect incorporation.[4–8] This can be detrimental for device performance, and addressing such issues requires modifying growth parameters and surface preparation from what is optimal for growths along the Ga-polar direction.

Alternatively, for vertical Ga-polar p-n structures, the built-in field direction with respect to the direction of current flow can be changed by simply reversing the order of the p- and n-type layers. But, due to extremely low p-type layer conductivity and the need for p-type activation, which occurs only through a bare surface or sidewalls, the viability of such structures remains limited. To increase the usefulness a new approach is needed.

To obtain p-type conductivity without the need of activation, a Hydrogen-free growth technique can be used. For growing buried tunnel junctions (TJs), plasma-assisted molecular beam epitaxy (PAMBE) is an attractive choice since with this method, the active region and the TJ can both be grown in the same process without transferring the sample between reactors.[9] Also, using PAMBE, comparing structures with the TJ grown before and after the active region is more reliable.[10]

Experimental

All structures investigated in this report were grown by PAMBE. All metals were supplied using standard k-cells, while active Nitrogen was supplied by a Veeco RF-plasma source. To assure the same growth temperature for all equivalent layers, metal-desorption time measurements of reference In and Ga fluxes were performed before the growth.

Fig. 1 schematically summarizes the LED structures utilizing tunnel junctions with: (a) top-TJ (TTJ) and (b) bottom-TJ (BTJ) designs. Fig. 1c shows the layer structure of a laser diode (LD) using the BTJ design. For clarity, in Fig. 1, the TJ and traditional LED (LD) regions are indicated. Rather thick (80+60 nm) InGaN layers near the quantum well are used in the LD structure to confine the optical mode in the vicinity of the active region of the device. For the LEDs, similar layers are used to minimize changes between the LED and LD growth conditions. In all cases, commercially available bulk Ga-polar n-type GaN substrates with $2-5 \cdot 10^{18} atoms/cm^3$ Oxygen doping were used. The InGaN layers were grown at 650–660°C, while the GaN and AlGaN layers were grown at 730–740°C. The compositions of the InGaN and AlGaN alloys were tuned using Ga and Al fluxes[11,12] only. GaN:Si layers were doped with $1 \cdot 10^{19} atoms/cm^3$, while the doping in the InGaN layers was $5 \cdot 10^{19} atoms/cm^3$ (InGaN:Si+) and $1 \cdot 10^{20} atoms/cm^3$ (InGaN:Si++). Similarly, GaN:Mg layers were doped with $5 \cdot 10^{18} atoms/cm^3$, InGaN:Mg+ doped with $5 \cdot 10^{19} atoms/cm^3$ and InGaN:Mg++ doped with $1 \cdot 10^{20} atoms/cm^3$. Doping levels between $5 \cdot 10^{18}$ and $5 \cdot 10^{19} atoms/cm^3$ were calibrated using secondary ion mass spectroscopy (SIMS) measurements. The higher doping level ($1 \cdot 10^{20} atoms/cm^3$) was estimated taking into account the lower growth rate used for those layers and, especially in the case of Mg doping, may be inaccurate. A GaN:UID (unintentionally doped) layer present only in the LD structure was grown to separate the optical mode from the highly absorptive Mg-doped layers. SIMS measurements performed on different structures with layers grown under similar conditions as the GaN:UID in the LD structure shown in Fig. 1c provide the background doping for every element: Oxygen, Silicon and Magnesium were all below $1 \cdot 10^{16} atoms/cm^3$.

LEDs with $100 \times 100\ \mu m^2$ area were then processed with common contacts on the back side of the substrate and separate contacts on top of each mesa. On-chip measurements were then performed using a probe station. The LD sample was processed into $5 \times 1000\ \mu m^2$ stripes with the same top and bottom metal contacts as the LEDs, with cleaved mirrors on both sides to form the Fabry-Perot cavity. LD chips were then mounted on copper clamps for better heat dissipation during measurements. The mesa etching depth for all LEDs and LDs was chosen to go through the entire structure, into the substrate.

Results

To illustrate the major advantage that BTJ LEDs (or p-up N-polar LEDs) have over standard Ga-polar p-up LEDs or TTJ LEDs, device

[z]E-mail: henryk@unipress.waw.pl

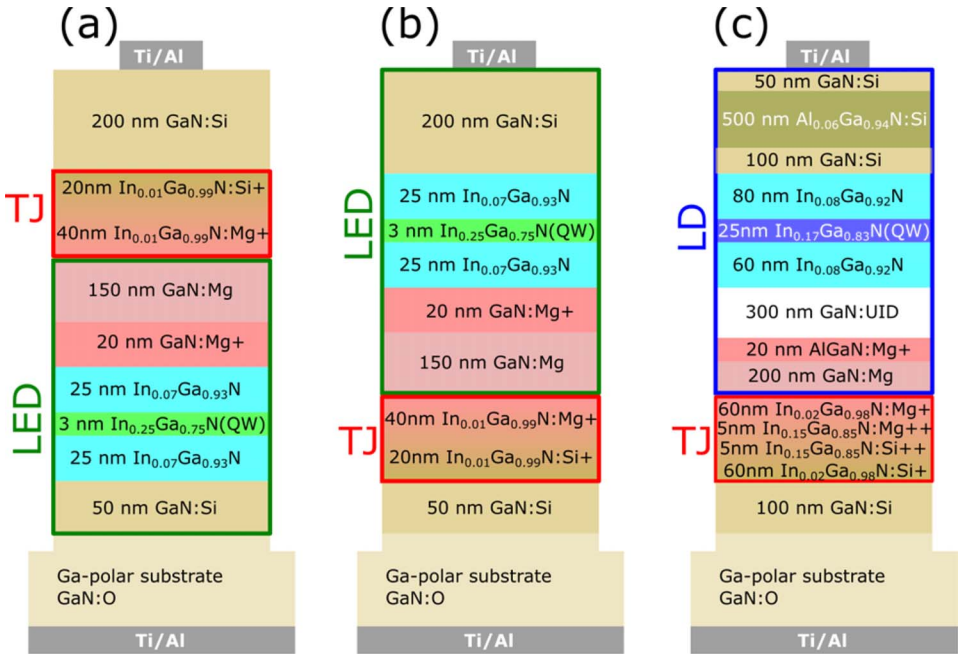

Figure 1. Layer structures of the (a) top-TJ LED, (b) bottom-TJ LED and (c) bottom-TJ LD structures obtained by PAMBE.

simulations using the SiLENSe package were performed. Energy band diagrams and carrier distributions near the quantum well for a current density of 20 A/cm^2 for the Ga-polar and N-polar LEDs are presented in Figs. 2a and 2b, respectively. For reference, a schematic structure is shown in the plot to mark changes in chemical compositions. Due to the difference in the built-in field direction between the Ga-polar LED (TTJ LED) and the N-polar LED (BTJ LED), the electron and hole concentrations are distributed in a qualitatively different way. For the standard Ga-polar (or TTJ) LEDs (see Fig. 2a), electrons and holes overflow past the QW and distribute in the p- and n-InGaN claddings, respectively. For the Ga-polar BTJ LED (or N-polar p-up LED) structures, on the other hand (Fig. 2b), the built-in electric field in the QW forms a natural energetic barrier for overflow of both electrons and holes. This leads to a situation where significant electron-hole overlap and recombination occurs only inside the QW. This highly desirable phenomenon increases injection efficiency by decreasing the magnitude of parasitic emission in the BTJ LED structure.

The expected decrease in parasitic electroluminescence channels between the TTJ (Fig. 1a) and BTJ (Fig. 1b) structures was experimentally observed as shown in Figs. 3a and 3b, respectively, for comparison. The electroluminescence spectra of the TTJ LED sample present a high energy emission peak (around 390 nm) next to the green emission from the QW. The corresponding spectra obtained for BTJ sample, on the other hand, only show a single peak from recombination in the QW, and higher overall emission intensity at higher current injection. The extra peak visible for the TTJ LED is from emission from $In_{0.07}Ga_{0.93}N$ cladding regions in the vicinity of the QW. As shown in Fig. 2a, significant carrier concentrations present in those regions lead to pronounced parasitic radiative recombination. A lack of parasitic recombination from layers surrounding the QW in the BTJ LED structure enables the possibility to make these layers thicker. Such thicker layer between the QW and the doped part of the laser diode structure (especially the p-type layers) would reduce optical losses generated by propagation of light in highly absorptive parts of the structure.

Blue-shifts in nitride quantum well structures in general are associated with built-in electric field screening and filling of localized low energy states originating from alloy composition fluctuations.[13] Thus, the difference in blue-shift magnitude observed for TTJ and BTJ LEDs could be another signature of higher injection efficiency for BTJ LEDs. More carriers may be present in the BTJ quantum well for the same current density, leading to stronger screening of the built-in field or filling of the localized states.

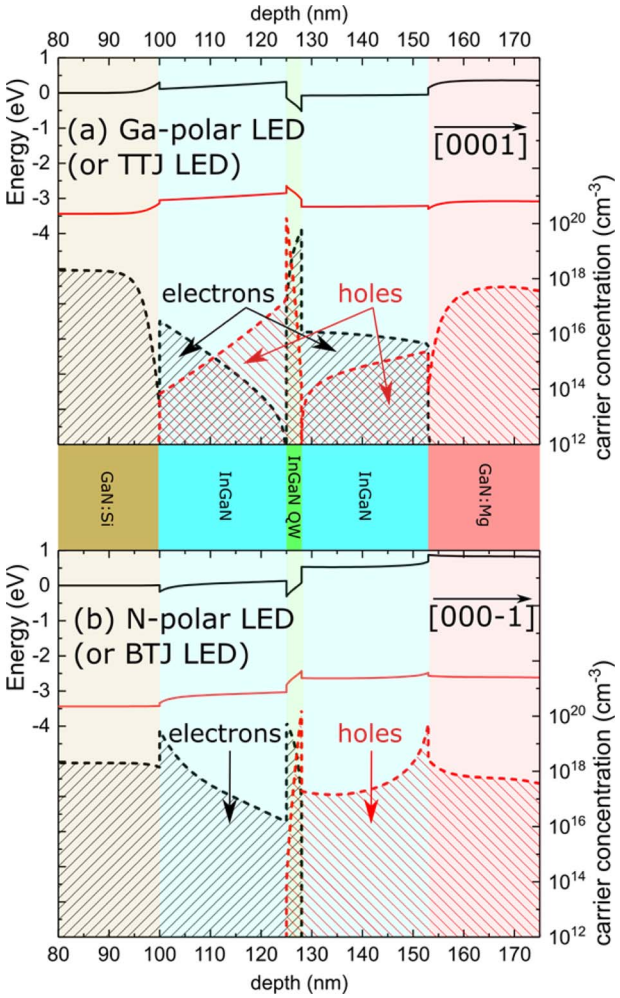

Figure 2. Numerical simulations of energy band diagrams and carrier distributions in the vicinity of the active region in LEDs for the (a) Ga- and (b) N-polar substrate orientations. The bottom figure is representative of what the energy bands would look like for a BTJ device on a Ga-polar substrate.

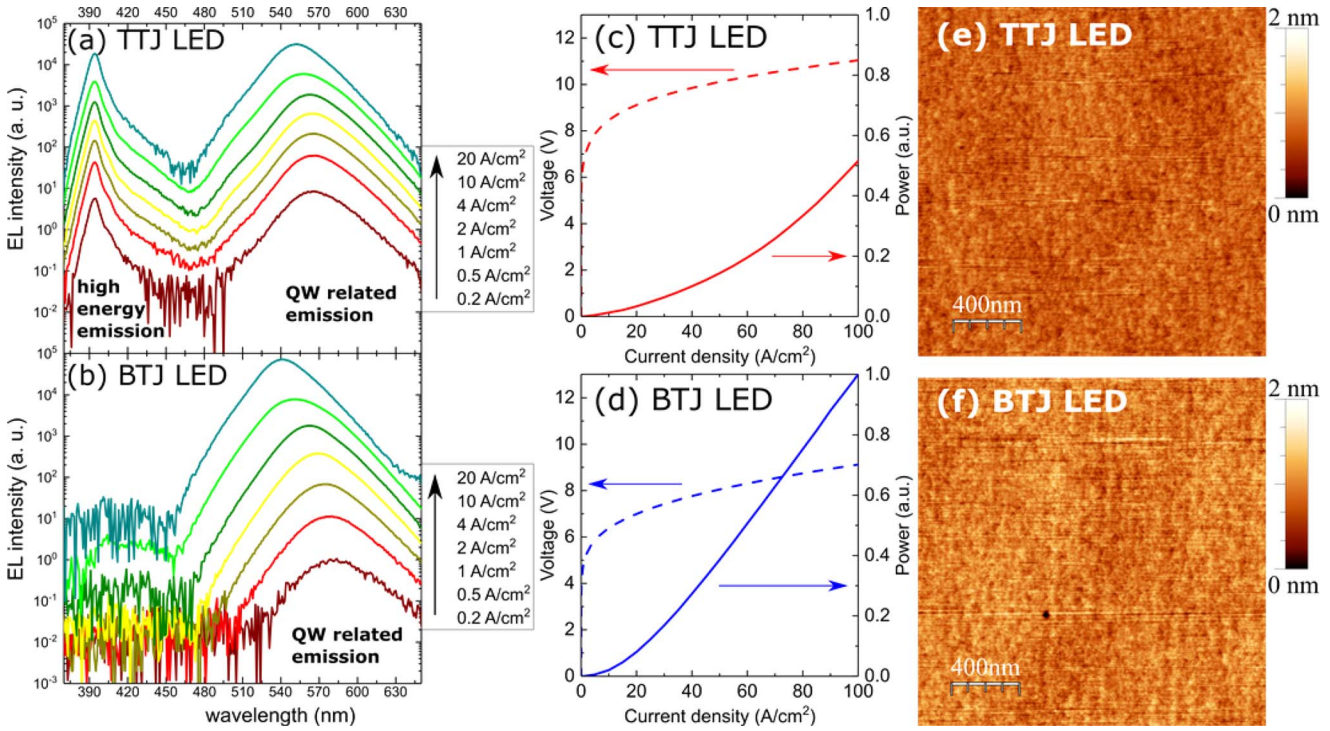

Figure 3. (a,b) Electroluminescence spectra, (c,d) light-current-voltage characteristics and (e,f) surface morphologies for green LEDs with (a,c,e) top- and (b,d,f) bottom-tunnel junction (TTJ and BTJ) constructions. Surface morphologies for the (e) TTJ and (f) BTJ structures exhibiting root mean square roughness of 0.16 nm and 0.19 nm, respectively, are shown.

To further demonstrate the higher efficiency of BTJ devices, in Figs. 3c, 3d, a comparison between light-current-voltage characteristics is shown where output power is presented in arbitrary units calculated as an integral of the whole emission spectra. Since both structures were measured on-chip, precise measurement of the total output power is challenging. The relative measurement indicates that the efficiency of the BTJ LED is higher by about 50% compared to the TTJ LED. The high operating voltage observed for both BTJ and TTJ devices is mainly caused by insufficient doping level in the TJ region for the structures presented in Figs. 1a, 1b. The doping was increased for the LD structure in Fig. 1c.

It is worth mentioning that at least part of the improvement in the overall emission intensity observed when moving from TTJ to BTJ LED designs may be associated with lower light absorption in layers above the active region. Existence of the high energy peak, together with the increase in the output power point to pronounced electron-hole overlap outside the QW for the TTJ LED structure.

To test the quality of both structures, atomic force microscopy (AFM) was used. As presented in Figs. 3e, 3f, smooth surface morphologies were seen for both structures, with low root mean square roughness values below 0.2 nm. This indicates that the extra peak in the spectra of the TTJ LEDs does not originate from large inhomogeneities during growth such as faceting.

To present a proof of concept that the BTJ approach can be used to obtain a laser diode, the structure presented in Fig. 1c was grown. A thick InGaN waveguide with an extra unintentionally doped GaN spacer was used to exploit the lack of parasitic recombination observed in the BTJ LEDs. The LD sample has an optimized TJ region with increased indium composition in the junction (to shrink the energy bandgap) and further increased concentration. Light-current-voltage

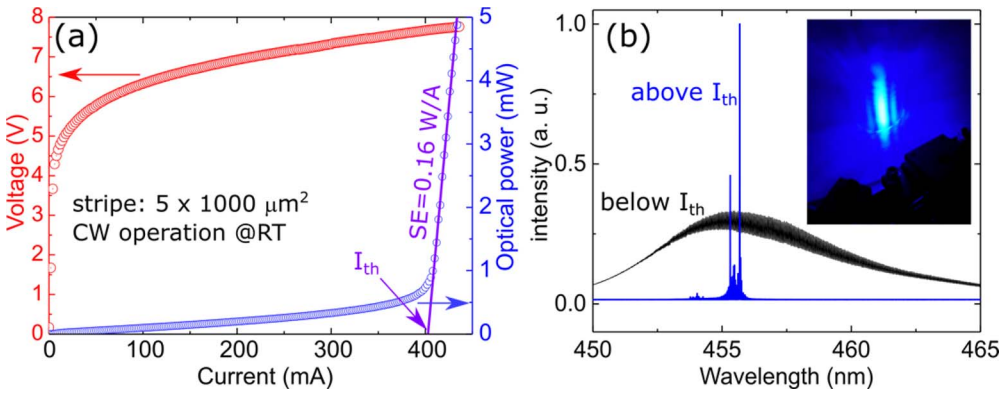

Figure 4. (a) Light-current-voltage characteristics for one of the first bottom-tunnel junction GaN laser diodes, exhibiting continuous wave operation at room temperature with threshold current around 400 mA and slope efficiency of 0.16 W/A. (b) High resolution electroluminescence spectra below (black) and above (blue) threshold. The inset in (b) shows the far-field pattern of the BTJ laser diode during operation.

characteristics from the obtained device are presented in Fig. 4a. A higher turn-on voltage was observed than that reported for the TTJ LDs by PAMBE.[14] This might be due to built-in fields in the TJ region that are in the opposite direction, which lead to a lower tunneling current for the same bias. A threshold current of 400 mA was observed. Further proof of lasing was obtained in the electroluminescence spectra observed above and below lasing threshold (Fig. 4b), and the far field pattern above threshold shown in the inset of Fig. 4b.

Discussion

Considerable efforts have been devoted to the growth of nitride nanowire devices utilizing TJs grown before the active region.[15,16] Only limited efforts have reported the growth of QW-based devices[9,10] with the TJ below the active region. Recent progress in the growth of stacks of LEDs and LDs by PAMBE[17] has now made it possible to realize GaN based LDs by utilizing the BTJ design for the first time.

PAMBE is an extremely interesting technology since it allows for the growth of p-type doped layers that do not need to be activated after growth. Furthermore, efficient active regions can be grown with the same epitaxial method, in contrast to ammonia MBE. As we present here, by showing the performance of BTJ LEDs and LDs, both regions (the heavily doped p-type layers in the TJ, and the high indium content QWs) can be grown on top of one another without structural degradation.

At the present stage of development, BTJ device performance falls behind that of the state-of-the-art structures obtained using traditional p-n arrangement. On the other hand, this approach offers a completely new way of controlling the built-in electric fields to our advantage to engineer carrier injection. BTJs allowed us to obtain the first LD with N-polar-like relationship between the built-in field and current flow, but on Ga-polar substrates. Due to the limitations in material quality for samples grown along the real [000-1] N-polar orientation, such devices have not been possible to be realized on substrates of that orientation to date.

To grasp the full potential of BTJ LDs and LEDs, further work on the optimization of the final layer structures is necessary. For example, parameters such as the thickness of the unintentionally doped GaN spacer, the mesa etching depth, and the growth parameters for the TJ region can still be improved.

Conclusions

Obtaining p-type conductivity by electron irradiation and next by thermal annealing was a technological breakthrough which launched the various applications for nitride photonic devices. In this work, we have presented a method by which Nitride photonic devices can be enriched, using the Hydrogen-free growth environment of PAMBE, in which no annealing procedure is needed to obtain p-type conductivity.

Devices utilizing buried p-type layers (stacks comprising a tunnel junction and light emitting region in the form of green LEDs and a blue LD) were realized. Comparisons of the emission spectra for TTJ and BTJ LEDs were shown. No parasitic electroluminescence was observed in the BTJ structures. For the TTJ device, the emission line associated with QW emission was accompanied by a higher energy emission peak due to recombination in layers surrounding the QW. This observation shows how built-in electric fields can be used to block carrier overflow and promote recombination only in the QW using the BTJ design.

To demonstrate the robustness of the BTJ design, a full electrically injected LD with TJ at the bottom was grown and processed. A thick unintentionally doped GaN spacer between the QW and p-type doped layers was used to benefit from the high injection efficiency of the BTJ design and to limit optical losses. Continuous wave operation of the BTJ LD at room temperature was achieved. Further improvement in the operating parameters is expected by optimizing the GaN spacer thickness, tunnel junction construction and mesa depth.

Acknowledgments

This work at Institute of High Pressure Physics was carried out within the Homing POIR.04.04.00-00-5D5B/18-00 and TEAM-TECH POIR.04.04.00-00-210C/16-00 projects of the Foundation for Polish Science co-financed by the European Union under the European Regional Development Fund and by the Polish National Centre for Research and Development grant LIDER/29/0185/L-7/15/NCBR/2016. The work at Cornell University was supported in part by the following National Science Foundation (NSF) grants: NSF DMREF Award No. 1534303 monitored by Dr. J. Schluter, NSF Award No. 1710298 monitored by Dr. T. Paskova, NSF CCMR MRSEC Award No. 1719875, and NSF RAISE TAQs Award No. 1839196 monitored by Dr. D. Dagenais. Characterizations and measurements were performed in part at the Cornell NanoScale Facility, a National Nanotechnology Coordinated Infrastructure member supported by NSF (grant ECCS-1542081); the Cornell Center for Materials Research Shared Facilities, supported through the NSF MRSEC program (DMR-1719875) and Major Research Instrumentation program (DMR-1338010).

ORCID

Henryk Turski https://orcid.org/0000-0002-2686-9842
Marcin Siekacz https://orcid.org/0000-0002-2359-8813
Grzegorz Muzioł https://orcid.org/0000-0001-7430-3838
Mateusz Hajdel https://orcid.org/0000-0001-9732-6119
Szymon Stańczyk https://orcid.org/0000-0001-8777-8947
Mikołaj Chlipała https://orcid.org/0000-0001-9922-0174
Czeslaw Skierbiszewski https://orcid.org/0000-0002-4718-4607
Shyam Bharadwaj https://orcid.org/0000-0002-6558-9835
Huili Grace Xing https://orcid.org/0000-0002-2709-3839
Debdeep Jena https://orcid.org/0000-0002-4076-4625

References

1. I. Akasaki, *Reviews of Modern Physics*, **87**, 1119 (2015).
2. H. Amano, *Reviews of Modern Physics*, **87**, 1133 (2015).
3. S. Nakamura, *Reviews of Modern Physics*, **87**, 1139 (2015).
4. C. Lund, S. Nakamura, S. P. DenBaars, U. K. Mishra, and S. Keller, *Semiconductor Science and Technology*, **34**, 075017 (2019).
5. F. Tuomisto, K. Saarinen, B. Lucznik, I. Grzegory, H. Teisseyre, T. Suski, S. Porowski, P. R. Hageman, and J. Likonen, *Applied Physics Letters*, **86**, 031915 (2005).
6. D. L. Becerra, D. A. Cohen, S. Mehari, S. P. DenBaars, and S. Nakamura, *Journal of Crystal Growth*, **507**, 118 (2019).
7. P. Shan Hsu, M. T. Hardy, F. Wu, I. Koslow, E. C. Young, A. E. Romanov, K. Fujito, D. F. Feezell, S. P. DenBaars, J. S. Speck, and S. Nakamura, *Applied Physics Letters*, **100**, 021104 (2012).
8. R. M. Farrell, E. C. Young, F. Wu, S. P. DenBaars, and J. S. Speck, *Semiconductor Science and Technology*, **27**, 024001 (2012).
9. M. J. Grundmann and U. K. Mishra, *Phys Status Solidi C*, **4**, 2830 (2007).
10. H. Turski, S. Bharadwaj, H. Xing, and D. Jena, *Journal of Applied Physics*, **125**, 203104 (2019).
11. H. Turski, M. Siekacz, M. Sawicka, Z. R. Wasilewski, S. Porowski, and C. Skierbiszewski, *Japanese Journal of Applied Physics*, **52**, 08JE02 (2013).
12. H. Turski, G. Muzioł, M. Siekacz, P. Wolny, K. Szkudlarek, A. Feduniewicz-Żmuda, K. Dybko, and C. Skierbiszewski, *Journal of Crystal Growth*, **482**, 56 (2018).
13. K. Kojima, M. Funato, Y. Kawakami, S. Nagahama, T. Mukai, H. Braun, and U. T. Schwarz, *Applied Physics Letters*, **89**, 241127 (2006).
14. C. Skierbiszewski, G. Muziol, K. Nowakowski-Szkudlarek, H. Turski, M. Siekacz, A. Feduniewicz-Zmuda, A. Nowakowska-Szkudlarek, M. Sawicka, and P. Perlin, *Applied Physics Express*, **11**, 034103 (2018).
15. A. T. M. G. Sarwar, B. J. May, J. I. Deitz, T. J. Grassman, D. W. McComb, and R. C. Myers, *Applied Physics Letters*, **107**, 101103 (2015).
16. S. M. Sadaf, Y. H. Ra, H. P. Nguyen, M. Djavid, and Z. Mi, *Nano Lett.*, **15**, 6696 (2015).
17. M. Siekacz, G. Muziol, M. Hajdel, M. Zak, K. Nowakowski-Szkudlarek, H. Turski, M. Sawicka, P. Wolny, A. Feduniewicz-Zmuda, S. Stanczyk, J. Moneta, and C. Skierbiszewski, *Opt. Express*, **27**, 5784 (2019).